DØ Note 5644-CONF

Search for First-Generation Leptoquarks in the dielectron channel with the DØ Detector in $p\bar{p}$ Collisions at $\sqrt{s} = 1.96$ TeV

The DØ Collaboration
URL http://www-d0.fnal.gov
(Dated: June 17, 2008)

A search for direct production of first-generation leptoquarks (LQ) is performed with $\sim$1 fb^{-1} of data collected by the DØ experiment in $p\bar{p}$ collisions at $\sqrt{s} = 1.96$ TeV at the Fermilab Tevatron collider. The topology analyzed consists of two electrons and two light-quark jets. We find our data consistent with standard model expectations, and set a 95% CL lower limit of 292 GeV on a scalar LQ mass and lower limits on vector LQ masses with different couplings from 350 to 458 GeV, for a branching fraction into an electron and a quark $\beta = 1$, improving the results obtained with a lower luminosity sample from Run II of the Tevatron.

Preliminary Results for Summer 2008 Conferences

I. INTRODUCTION

Leptoquarks (LQ) are massive particles predicted by many extensions[1] of the Standard Model. In such exotic models, transitions between the leptonic and baryonic sectors would be allowed. Thereby, the detection of leptoquarks could be, among others, the signature of compositeness, supersymmetric couplings in RPV scenarios, Grand Unification models or technicolor.

At the Tevatron, leptoquarks are dominantly produced by strong interactions between the proton and antiproton constituents. The branching fraction β is defined for the LQ or $\overline{LQ}$ decay into a charged lepton and a quark. $1-\beta$ is the branching fraction of the reaction $LQ \to \nu + q$. In the analysis considered here, limits are set on the product of the cross section times β^2 and used to set a limit on the LQ masses for the case $\beta^2 = 1$. In this paper, we describe the dielectron channel analysis in which both LQ decay into an electron and a light quark. The topology of the events for this process corresponds to a final state with two electrons and two jets.

In previous analyses of a $\sim$250 pb^{-1} data sample [2, 3] (a subset of the luminosity presented in this paper), the CDF and DØ collaborations have set a limit on the mass of the first-generation scalar leptoquark at $\sim$240 GeV assuming $\beta^2 = 1$.

This study is performed on data collected with the DØ detector [4] during Run IIa of the Tevatron. The DØ detector comprises three main elements. A magnetic central-tracking system, which consists of a silicon microstrip tracker and a central fiber tracker, is located within a 2 T superconducting solenoidal magnet. Three liquid-argon/uranium calorimeters, a central section (CC) covering pseudorapidities $|\eta|$ up to $\simeq 1$ and two end calorimeters (EC) extending coverage to $|\eta| \simeq 4$, are housed in separate cryostats. Scintillators between the CC and EC cryostats provide a sampling of developing showers for $1.1 < |\eta| < 1.4$. A muon system is located outside the calorimeters.

II. DATA SAMPLE AND SIMULATED EVENTS

The data sample consists of 36M events with at least two electromagnetic (EM) objects of $p_T > 12$ GeV.
The total integrated luminosity for unprescaled EM triggers is 1.02 fb^{-1}.

The standard model (SM) backgrounds relevant to our analysis comprise $Z/\gamma^* \to e^+e^-$, $\tau^+\tau^-$, top pairs in dileptonic channels, and di-bosons produced together with jets. Additionally, an instrumental background consists of multijet processes. The dibosons processes were generated with PYTHIA [5] while the other SM processes were generated with ALPGEN [6] and interfaced with PYTHIA. The parton density function (PDF) used is `CTEQ6L1` [7, 8]. NLO cross sections for ALPGEN generator are derived using K-factor by comparison of LO and NLO cross section in MCFM [9].

The p_T spectrum of the Z boson from ALPGEN samples does not correctly reproduce the distribution observed in data and therefore a reweighting procedure is used. The SM generated backgrounds events are normalized to the data luminosity. The ALPGEN inclusive W/Z production is normalized to the NLO theoretical prediction.

An important background in this channel is of an instrumental nature. It is due to the misidentification of jets as electrons. Four-jet events can thus be reconstructed as *eejj* events. This multijet contribution is not properly simulated and therefore is extracted from the data.

The LQs can either be scalar or vector fields. Scalar and vector LQ samples have been generated using PYTHIA and COMPHEP [10] respectively, both with `CTEQ6L1` parton density functions. We have simulated events for scalar LQs in a range of 120 to 320 GeV in steps of 10 or 20 GeV. A full detector simulation based on GEANT package [11] and event reconstruction has been performed. Next-to-Leading Order (NLO) cross sections of scalar leptoquarks pair production have been determined in [12].

To generate the vector leptoquarks, the model described in reference [13] and implemented in COMPHEP is used. There are many species of vector LQs, with different isospin (T_3), electrical charge (Q_{em}) and LQ-quark-lepton couplings. In this analysis we have generated pairs of "VM-type" leptoquarks: $T_3 = -1/2$, $Q_{em} = +1/3$, and a LQ-quark-lepton coupling $\lambda_{eff} = e$. In this model, the cross section depends on the LQ mass and on the "anomalous" couplings κ_G and λ_G. In the following, three types of couplings have been considered: $\{\kappa_G = 1,\ \lambda_G = 0\}$ (Minimal Coupling or MC), $\{\kappa_G = 0,\ \lambda_G = 0\}$ (Yang-Mills coupling or YM) and $\{\kappa_G = -1,\ \lambda_G = -1\}$ (Minus Minus coupling or MM). A full simulation and event reconstruction has been performed. We use LO cross sections given by COMPHEP.

III. EVENT SELECTION

All data events have been required to fulfill the following conditions. Events must pass one of the triggers on a single object in the electromagnetic calorimeter. An electron-trigger matching is performed to check which electron fired the trigger [15]. Events must have at least 2 "tight" electron candidates with the following criteria: 90% of the

clustered energy deposited in the EM sections of the calorimeter, an isolation in the calorimeter ≤ 0.15 [16], a track with $p_T > 5$ GeV, and an electron likelihood value ≥ 0.85 using a shower shape parameter and the number of tracks in the vicinity of the electron. Electrons must have $p_T > 25$ GeV and be detected in $|\eta_{det}| < 1.1$ (CC) or $1.5 < |\eta_{det}| < 2.5$ (EC). To maintain a good reconstruction efficiency, we require at least one EM in the central calorimeter (CC). The primary vertex must have $|z| < 60$ cm, at least 3 associated tracks, and the projection of the electron tracks to the vertex within $|\Delta z| < 1$ cm.

We select events with at least one jet reconstructed in a cone of radius $\mathcal{R} = 0.5$ ($\mathcal{R} = \sqrt{(\Delta\eta)^2 + (\Delta\phi)^2}$), with $p_T > 25$ GeV and in $|\eta_{det}| < 2.5$, and at a minimal distance $\mathcal{R} > 0.5$ from any EM object. Jet energies are corrected to the particle level. The jet energy scale is corrected so as to take into account the presence of muons in the jet. The muons in $|\eta| < 2.0$ are matched with the jets within a maximal distance $\mathcal{R} = 0.5$. Events with isolated muons with $p_T > 15$ GeV and $|\eta| < 2.0$ are removed from the sample.

In order to model the multijet contribution, a specific sample containing events with 2 "fake electrons" and ≥ 1 additional jet is created. The fake electrons are isolated in the calorimeter, have a usual EM fraction value, but shower shape conditions opposite to the signal. They are also required to have $p_T > 25$ GeV, and be detected in the CC or EC.

Data and Monte Carlo samples have passed the same selection criteria. But since the efficiency of these selection cuts is different for data and for MC, efficiency corrections have to be applied to the simulated events: the trigger probability (η_{det} and p_T-dependent efficiencies for the chosen single electron triggers), a correction for the efficiencies of the jet selection, and an η_{det} and ϕ_{det}-dependent correction of the electron selection (EMID) efficiency. The samples are normalized on the dielectron invariant mass distribution (M_{ee}) via a matrix method. Two regions of the M_{ee} spectrum are considered: $50 < M_{ee} \leq 80$ GeV and $80 < M_{ee} \leq 102$ GeV. The normalization factors are computed by solving the following equation in these two regions :

$$Data_i = k_Z * (Z_i) + k_{MJ} * (MJ_i) + EW_i \qquad\qquad i = \{1, 2\}$$

where $Data_i$ is the number of data events in region i, Z_i is the number of Monte Carlo Z+jets backgrounds, EW_i is the number of the other Monte Carlo SM backgrounds and MJ_i is the number of multijet events in this region. Table I summarizes the number of events of all the samples when using the normalization factors, first at the level of the normalization (≥ 1 jet) and after the requirement of a second jet with $p_T > 25$ GeV.

TABLE I: Number of events after normalization in the data and background samples, and expected signal for a scalar LQ with $M_{LQ} = 250$ GeV.

Sample	# events ≥ 1 jet	# events ≥ 2 jets
Data	4009	448
$Z/\gamma^* \rightarrow ee$	3909.5 $\pm$ 80.4	410.6 $\pm$ 9.7
$Z/\gamma^* \rightarrow \tau\tau$	6.3 $\pm$ 1.0	0.4 $\pm$ 0.1
$t\bar{t} \rightarrow 2l2\nu2b$	13.3 $\pm$ 0.1	8.5 $\pm$ 0.1
Dibosons	28.8 $\pm$ 0.4	11.7 $\pm$ 0.2
Multijet	115.6 $\pm$ 63.2	17.1 $\pm$ 9.4
Total background	4074.5 $\pm$ 102.3	449.3 $\pm$ 13.4
Signal $M_{LQ} = 250$ GeV	13.9 $\pm$ 0.2	11.9 $\pm$ 0.2

Data are compatible with SM expectations, even after adding the requirement of a second jet. Fig. 1 shows the distributions of dielectron invariant mass and S_T, the transverse scalar energy defined as the sum of the transverse momentum of the two leading electrons and two leading jets. The signal for a scalar LQ with $M_{LQ} = 250$ GeV has been superimposed.

The effect of the sequential cuts on the data events and on the scalar LQ sample for $M_{LQ} = 250$ GeV is summarized in Table II. The acceptance of a given cut **Ci** is calculated relatively to cut **Ci-1**. The most important cutoffs of **C0** are the requirement of a good jet with $p_T > 15$ GeV and tight criteria for both leading electrons. **C1** is applied with the aim of reducing the multijet background without altering the signal too much. With **C2**, we ask for events with at least one electron in the central calorimeter in order to maintain a good reconstruction efficiency. For **C3**, the jets must have $p_T > 25$ GeV and be in $|\eta| < 2.5$ (described earlier in this section). **C4** requires the events contain ≥ 2 tight electrons and ≥ 2 good jets, all coming from the same vertex. Finally, in order to remove the main source of background, the $Z(\rightarrow ee)$+jets processes, **C5**, $M_{ee} > 110$ GeV, is applied. This cut, which will be studied in section VI, is illustrated on Fig. 2 for two discriminant variables: M_{ee} and S_T. Fig. 2b shows that a noticeable part of the multijet background is restrained to the range $S_T < 300$ GeV.

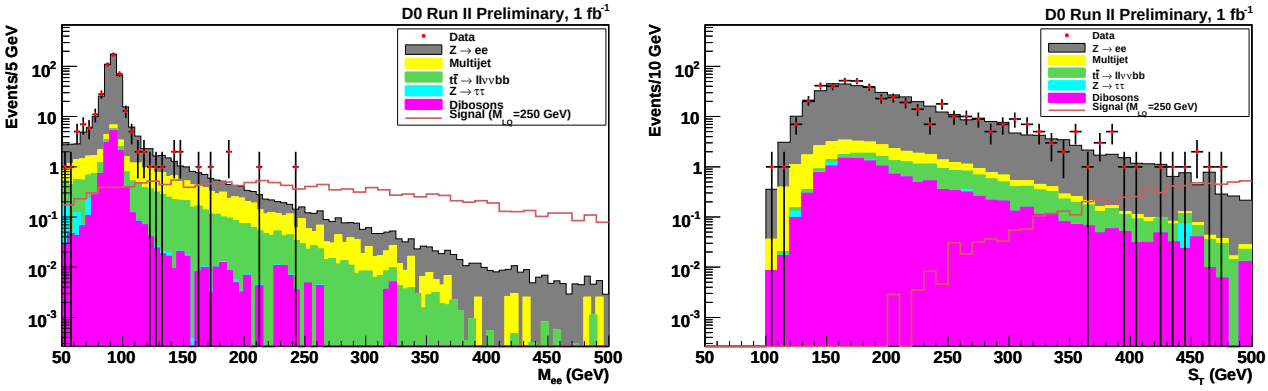

(a) (b)

FIG. 1: Dielectron invariant mass (a) and S_T (b) for events with ≥ 2 jets. The signal for a scalar LQ with $M_{LQ} = 250$ GeV has been superimposed.

TABLE II: Sequence of criteria applied for the selection, remaining events and acceptances for each cut relative to the previous on the data sample and for a signal corresponding to $M_{LQ} = 250$ GeV.

Cuts	Data events	Data accept.(%)	Signal accept.(%)
C0 : 2 electrons $p_T > 25$ GeV, $\geq$1 jet $p_T > 15$ GeV	10607	76.4	97.9
C1 : $+ M_{ee} > 50$ GeV	10518	99.2	97.9
C2 : $+ \geq 1$ electron in CC	9924	94.4	99.3
C3 : $+ \geq 1$ jet with $p_T > 25$ GeV	4009	40.4	99.9
C4 : $+ \geq 2$ jets with $p_T > 25$ GeV	448	11.2	85.6
C5 : $+ M_{ee} > 110$ GeV (Z veto)	17	3.8	87.4

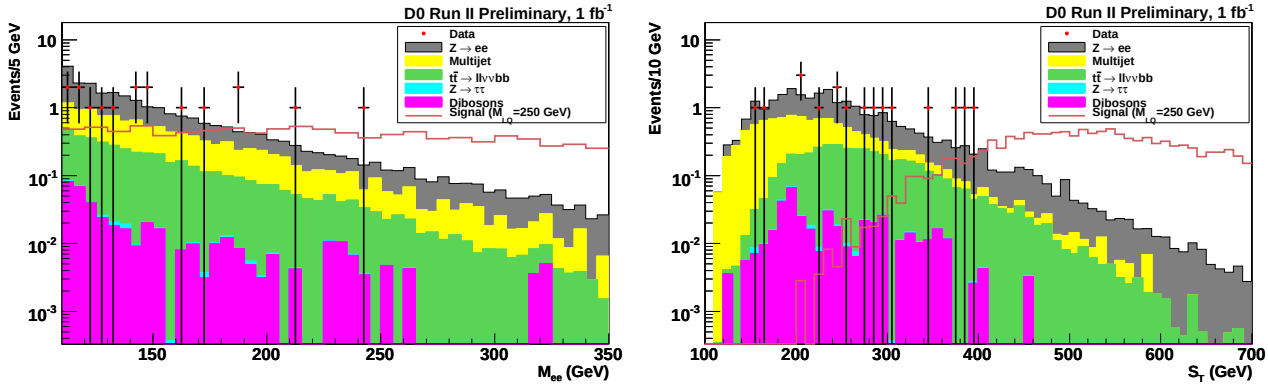

(a) (b)

FIG. 2: Dielectron invariant mass (a) and transverse scalar energy (b) distributions after requiring $M_{ee} > 110$ GeV. The signal for a scalar LQ with $M_{LQ} = 250$ GeV has been superimposed.

IV. SIGNAL ACCEPTANCE

The acceptance as a function of the selection criteria is shown in Fig. 3a for scalar LQs with a M_{LQ} from 210 to 320 GeV. From Fig. 2b, we take that a minimal cut at $S_T > 300$ GeV considerably reduces the backgrounds. The effect of the variation of this cut on the signal acceptance is shown in Fig. 3a and will further be discussed. In order to compare the acceptance of vector LQs to scalar LQs, we have generated events for the three couplings for $M_{LQ} = 250$ GeV. In Fig. 3b, the scalar case corresponds to the PYTHIA sample for $M_{LQ} = 250$ GeV shown in Fig. 3a. As illustrated on Fig. 3b, the relative acceptances of the selection criteria on the scalar and vector LQ samples for the same LQ mass are quite comparable. The small variations of acceptance are explained by differences in their M_{ee} and electron p_T spectra at the generator level.

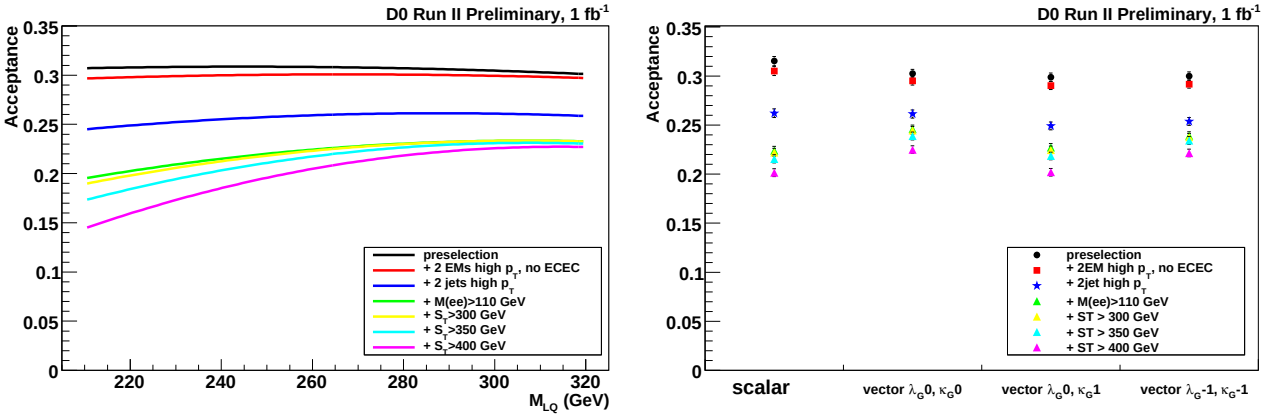

(a) (b)

FIG. 3: Acceptance of the selection criteria as a function of the scalar LQ mass (a) and for different types of LQs of mass 250 GeV (b). The statistical error on the acceptance is $< 2\%$.

V. SYSTEMATIC UNCERTAINTIES

Systematic uncertainties affect the acceptance of the signal and background events. The jet energy scale leads to $^{+1.7}_{-2.0}\%$ error on the SM background and $^{+0.1}_{-0.5}\%$ on the signal. The systematic uncertainty from the correction of the electron identification efficiency is evaluated on one hand, from the error on the correction factors themselves, and on the other hand, from the choice of another parameterization of the correction ($\pm 0.2\%$ of the SM background and $\pm 8\%$ of the signal). The error on the correction of the jet identification efficiency is estimated to be $\pm 0.4\%$ on SM background and $\pm 0.7\%$ on signal. The effect of the PDF choice on the signal acceptances ($\pm 5\%$ for $M_{LQ} = 250$ GeV) is determined by using a different PDF set (20-eigenvector basis `CTEQ6.1M` NLO PDF). The uncertainty on the LO cross sections used to merge the jet multiplicity bins of the ALPGEN samples is $^{+1.2}_{-1.1}\%$. The normalization of the background samples is based on a matrix method depending on the range of the two regions in the invariant mass spectrum; by varying the range of 5 GeV, we ended up with a difference of 1.2%. A $\pm 6.1\%$ uncertainty affects the luminosity.

VI. OPTIMIZATION AND LIMIT CALCULATION

A. Limit on the scalar LQ cross section

Table III presents the number of events in the total background samples for different values of M_{ee} and S_T. It also gives the number of events for a signal with $M_{LQ} = 290$ GeV and normalized to $\mathcal{L}_{data}$ with a σ_{NLO}. Cross section limits were set using the $< M_{ej} >= (M_{ej}1 + M_{ej}2)/2$ distributions (average of the two electron-jet invariant

TABLE III: Number of background and signal events for various cuts on the dielectron invariant mass and transverse scalar energy.

M_{ee} cut (GeV)	S_T cut (GeV)	Backgrounds	Signal NLO ($M_{LQ} = 290$ GeV)
105	350	3.03 ± 0.20 (stat) ± 0.08 (syst)	4.20 ± 0.08 (stat) ± 0.47 (syst)
110	350	2.87 ± 0.19 (stat) ± 0.08 (syst)	4.14 ± 0.08 (stat) ± 0.47 (syst)
105	400	1.63 ± 0.14 (stat) ± 0.04 (syst)	4.07 ± 0.07 (stat) ± 0.46 (syst)
110	400	1.51 ± 0.12 (stat) ± 0.04 (syst)	4.01 ± 0.07 (stat) ± 0.45 (syst)

masses which give the smallest difference between the LQ and $\overline{LQ}$ masses) and the TLimit tool [14], a frequentist CLs approach. The acceptances and the corresponding expected limit cross sections have been derived for each LQ mass and value of the cuts on M_{ee} (from 105 to 120 GeV) and S_T (from 300 to 500 GeV). Among the 20 cases we have studied, the only four best combinations ($M_{ee} > 105$, 110 GeV and $S_T > 350$, 400 GeV) are discussed here (see Fig. 4). We observed that the results for a high value of the LQ mass are very stable as the M_{ee} and S_T cuts vary. The cuts at $M_{ee} > 110$ GeV and $S_T > 400$ GeV give one of the lowest limit for high LQ mass values, and since these are the highest values of the M_{ee} and S_T cuts, the background in this case is minimum. As a consequence, this set of cuts will be used to determine the limit on the LQ mass. The distribution of $< Mej >$ for background and signal events (for $M_{LQ} = 290$ GeV) with $M_{ee} > 110$ and $S_T > 400$ GeV is presented on Fig. 5. No data events remain at this stage. Figure 6 shows the NLO theoretical cross sections and the 95% C.L. limit on the experimental cross section times β^2 as a function of the scalar LQ mass. For $\beta = 1$, the intersection of the lowest theoretical cross section (with a factorization and renormalization scale $\mu = 2M_{LQ}$) gives a limit on the scalar LQ mass of 292 GeV, and a mass of 299 GeV for $\mu = M_{LQ}$.

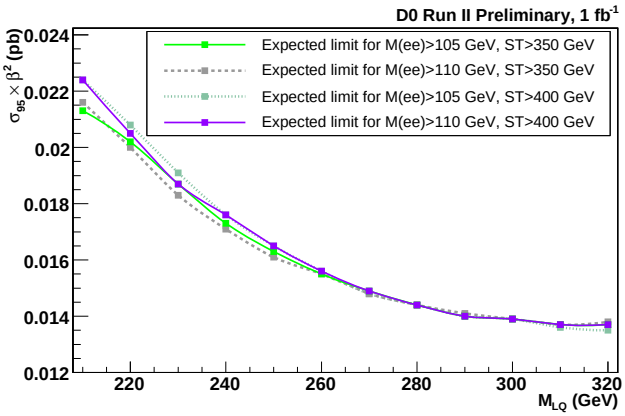

FIG. 4: 95% C.L. limit on the experimental cross section times branching ratio as a function of the scalar LQ mass.

B. Limit on the vector LQ cross section

To compute the limit on vector LQ cross sections, the data, background and signal acceptances have been used as input for TLimit, with cuts applied on M_{ee} at 110 GeV and for various S_T cuts. We determined the acceptances for each vector LQ coupling using events generated with a LQ mass of 250 GeV. As the acceptances of the selection criteria on the scalar and vector LQ samples for the same LQ mass are quite comparable, and that in the scalar case, the acceptance increases with the LQ mass, we assumed that the vector LQ acceptances have the same behaviour. Therefore, we use conservatively in the limit calculus, acceptances of samples generated for a mass of 250 GeV. Moreover, we use the same systematics as in the scalar case. After applying the cuts, and for each S_T value, the number of data, total expected background events and the acceptance for each VM coupling are given in Table IV with the expected limit cross sections at 95% C.L. The best expected limit cross section, for every coupling, corresponds to the S_T cut at 400 GeV. Figure 6 shows the theoretical cross sections for the three couplings together with the observed and expected cross sections. The limits on M_{LQ} are determined in the same manner as for scalar LQs and

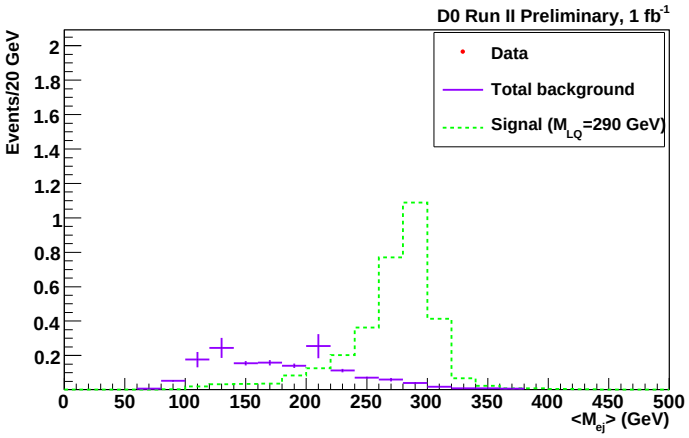

FIG. 5: Distribution of the variable $< Mej >$ for background and signal events (for $M_{LQ} = 290$ GeV) with $M_{ee} > 110$ and $S_T > 400$ GeV. No data events remain at this stage.

are summarized in Table V. For $\beta = 1$, a limit on the vector LQ mass with MC coupling is set at 350 GeV with $\mu = 2M_{LQ}$ and at 361 GeV for $\mu = M_{LQ}$. For a YM vector coupling, a limit on the LQ mass is set a 410 GeV with $\mu = 2M_{LQ}$ and 421 GeV for $\mu = M_{LQ}$. For a MM coupling, vector LQs with a mass less than 458 GeV (with $\mu = 2M_{LQ}$) or with a mass less than 467 GeV (with $\mu = M_{LQ}$) are excluded.

TABLE IV: Expected limit cross sections for vector Leptoquark (VM) pair production for the three types of couplings and different values of the S_T cut. The errors given are statistical uncertainties.

S_T cut (GeV)	> 300	> 350	> 400	> 450	> 500
data	5	3	0	0	0
background	5.27 ± 0.35	2.87 ± 0.19	1.51 ± 0.12	0.79 ± 0.08	0.35 ± 0.02
MM acceptance (%)	23.8 ± 0.4	23.4 ± 0.4	22.2 ± 0.4	19.9 ± 0.4	16.8 ± 0.3
MM exp. σ_{95} (pb)	0.026	0.024	0.018	0.021	0.018
MM obs. σ_{95} (pb)	0.026	0.024	0.013	0.015	0.018
YM acceptance (%)	24.4 ± 0.4	23.9 ± 0.4	22.5 ± 0.4	19.9 ± 0.4	16.6 ± 0.3
YM exp. σ_{95} (pb)	0.025	0.023	0.018	0.021	0.018
YM obs. σ_{95} (pb)	0.026	0.023	0.013	0.015	0.018
MC acceptance (%)	22.5 ± 0.4	21.9 ± 0.4	20.2 ± 0.4	17.4 ± 0.3	13.9 ± 0.3
MC exp. σ_{95} (pb)	0.027	0.025	0.020	0.024	0.022
MC obs. σ_{95} (pb)	0.027	0.025	0.015	0.017	0.022

TABLE V: Mass limits in GeV for Vector Leptoquark (VM) pair production for three couplings and $S_T > 400$ GeV.

Coupling	Mass limit from exp. σ_{95}	Mass limit from obs. σ_{95} and $\mu = 2M_{LQ}$	Mass limit from obs. σ_{95} and $\mu = M_{LQ}$
MM	448	458	467
YM	400	410	421
MC	340	350	361

VII. CONCLUSION

We have analyzed a sample of eejj events corresponding to a luminosity of 1.02 fb^{-1}. The number of observed events agree with background expectations and we have set limits on the cross section times branching fraction squared for the production of scalar and vector leptoquark pairs decaying to the e+jet final state as a function of the leptoquark mass. The limits are interpreted as mass limits and exclude leptoquarks with masses less than 292 GeV for scalar leptoquarks and from 350 to 458 GeV for vector leptoquarks, depending on the coupling.

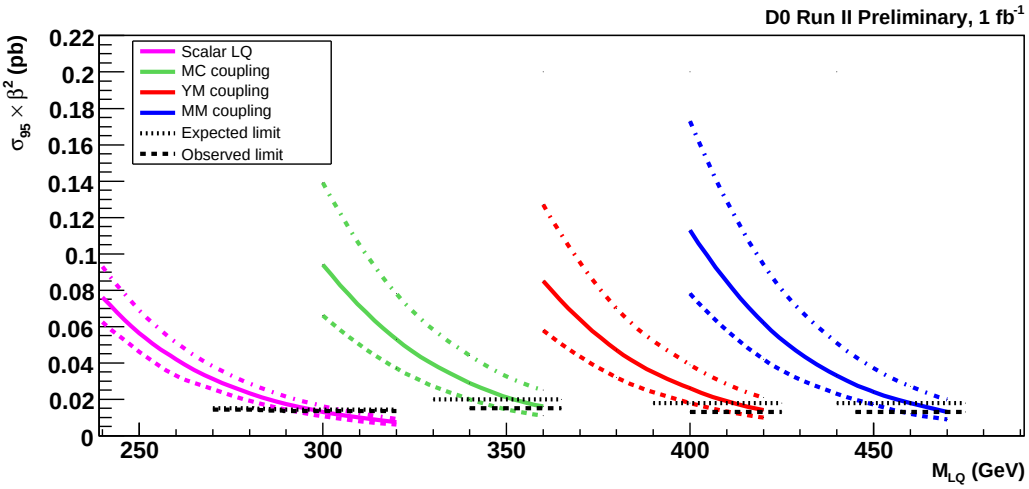

FIG. 6: Cross sections as a function of the vector LQ mass for the three different couplings. The LO (vector LQ) or NLO (scalar) theoretical cross sections are drawn for different values of the renormalization scale: M_{LQ} (solid line), $M_{LQ}/2$ (dot-dashed line) and $2M_{LQ}$ (dashed line). The horizontal black lines correspond to the expected limit cross section (dotted line) and the observed limit cross section (dashed line) for each coupling.

Acknowledgments

We thank the staffs at Fermilab and collaborating institutions, and acknowledge support from the DOE and NSF (USA); CEA and CNRS/IN2P3 (France); FASI, Rosatom and RFBR (Russia); CAPES, CNPq, FAPERJ, FAPESP and FUNDUNESP (Brazil); DAE and DST (India); Colciencias (Colombia); CONACyT (Mexico); KRF (Korea); CONICET and UBACyT (Argentina); FOM (The Netherlands); PPARC (United Kingdom); MSMT (Czech Republic); CRC Program, CFI, NSERC and WestGrid Project (Canada); BMBF and DFG (Germany); SFI (Ireland); Research Corporation, Alexander von Humboldt Foundation, and the Marie Curie Program.

[1] D. Acosta and S.K. Blessing, Ann. Rev. Nucl. Part. Sci. **49**, 389 (1999) and references therein;
W.-M. Yao *et al.*, J. Phys. G **33**, 1 (2006) and 2007 partial update for the 2008 edition available on the PDG WWW pages (URL: http://pdg.lbl.gov/)
[2] V.M. Abazov *et al.* (DØ Collaboration), Phys. Rev. D **71**, 071104(R) (2005).
[3] D. Acosta *et al.* (CDF Collaboration), Phys. Rev. D **72**, 051107 (2005).
[4] V.M. Abazov *et al.* (DØ Collaboration), Nucl. Instrum. Methods A **565**, 463 (2006).
[5] T. Sjöstrand *et al.*, *PYTHIA 6.2 Physics and Manual*, http://citeseer.ist.psu.edu/626868.html
[6] M.L. Mangano *et al.*, JHEP **07**, 001 (2003).
[7] H.L. Lai *et al.* (CTEQ Collaboration), Eur. Phys. J. C **12**, 375 (2000) and references therein.
[8] J. Pumplin *et al.*, JHEP **07**, 012 (2002);
D. Stump *et al.*, JHEP **10**, 046 (2003).
[9] J. Campbell and K. Ellis, *MCFM - Monte Carlo for FeMtobarn processes*, http://mcfm.fnal.gov/
[10] A. Pukhov *et al.*, arXiv:hep-ph/9908288 (1999);
E. Boos *et al.* (CompHEP Collaboration), Nucl. Instrum. Methods A **534**, 250 (2004).
[11] R. Brun and F. Carminati, CERN Program Library Long Writeup W5013, 1994.
[12] M. Kramer *et al.*, Phys. Rev. Lett. **79**, 341 (1997).
[13] A. Belyaev *et al.*, JHEP **09**, 005 (2005).
[14] http://root.cern.ch/root/html/TLimit.html
[15] At high electron p_T values, the trigger efficiency is very close to 100%. Nevertheless, the trigger efficiency has been applied to the simulation.
[16] The energy cluster must be isolated from other energy deposits in the calorimeter. The fraction of energy in an annular isolation cone of radius $0.2 < \mathcal{R} < 0.4$ must be less than 15% of the energy in the core cone of radius $\mathcal{R} < 0.2$.

Appendix

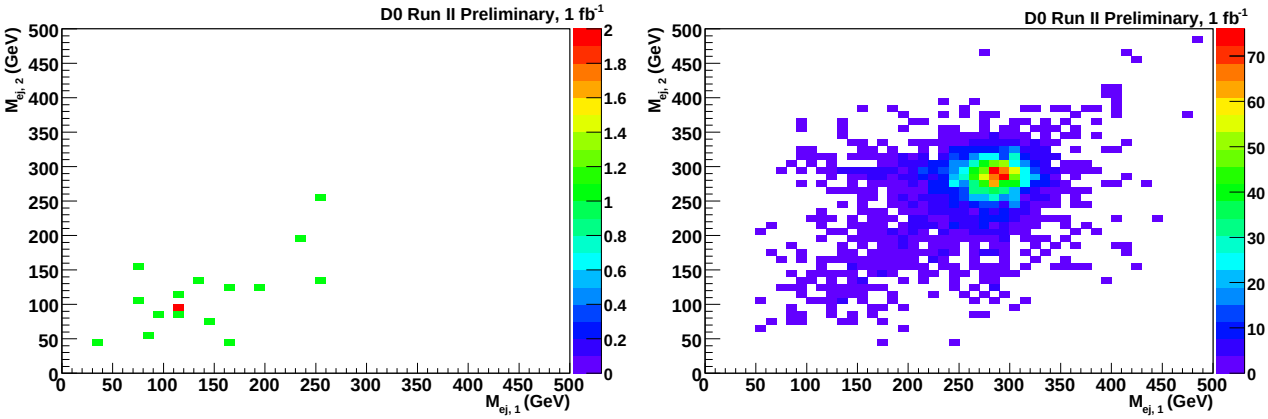

FIG. 7: $M_{ej}1$ versus $M_{ej}2$ at the level of **C5** for the data events (left) and signal with $M_{LQ} = 290$ GeV (right).

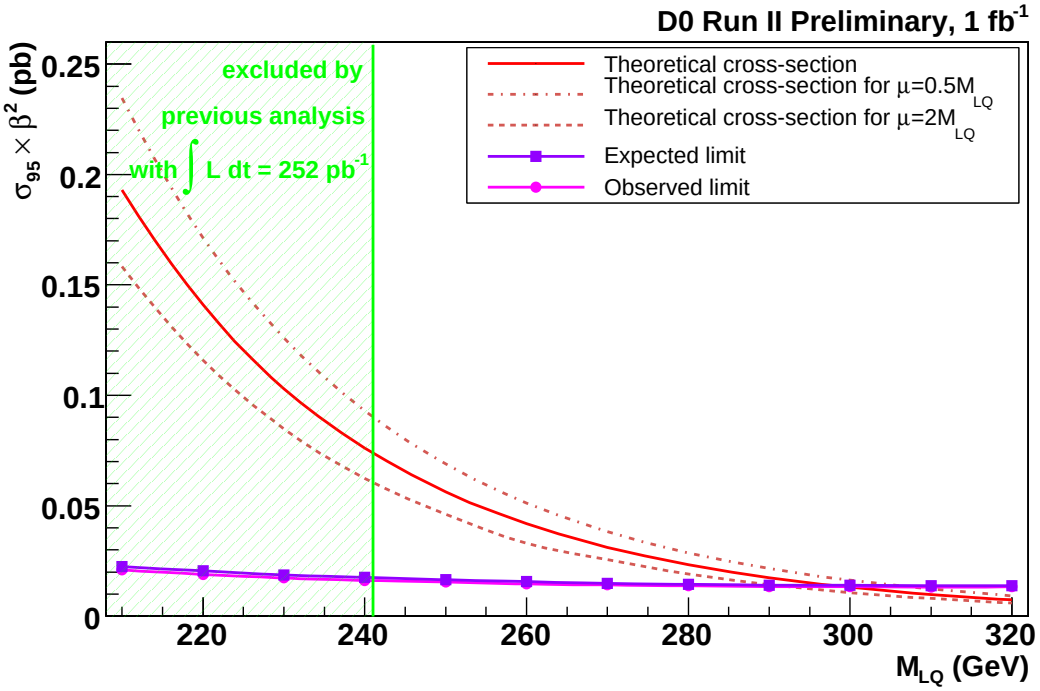

FIG. 8: 95% C.L. limit on the experimental cross section times branching fraction as a function of the scalar LQ mass. The NLO theoretical cross sections are plotted for different values of the renormalization scale factor: M_{LQ} (solid line), $M_{LQ}/2$ (dot-dashed line) and $2M_{LQ}$ (dashed line), taking into account the PDF uncertainties. A limit on the scalar LQ mass of 292 GeV is obtained for $\beta = 1$ and $\mu = 2M_{LQ}$.

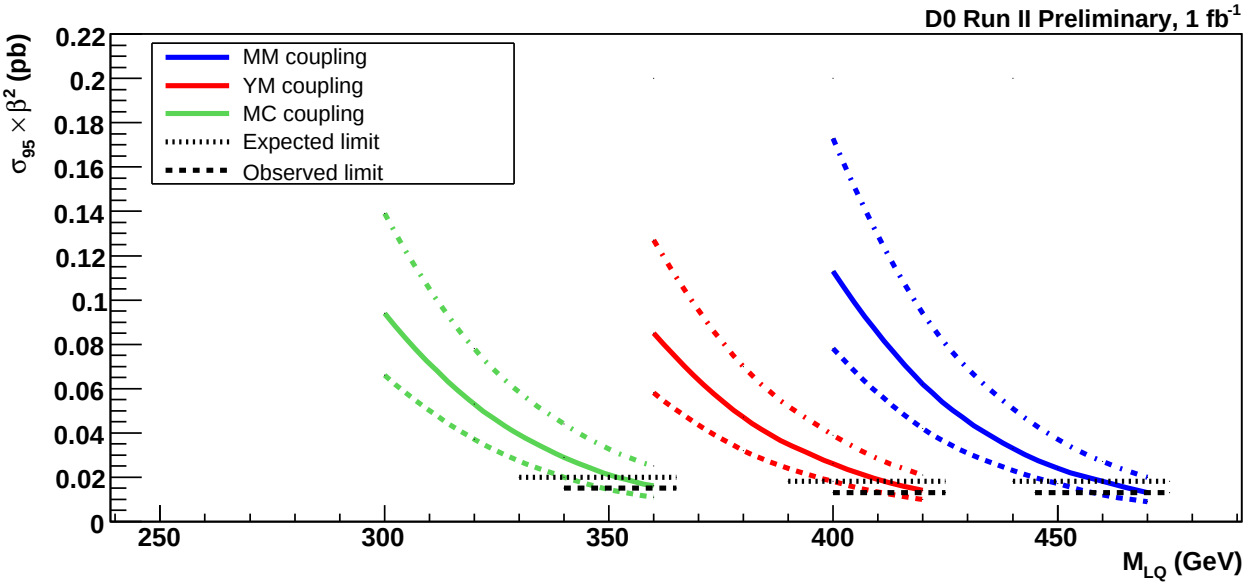

FIG. 9: Cross sections as a function of the vector LQ mass for the three different couplings. The LO theoretical cross sections are drawn for different values of the renormalization scale: M_{LQ} (solid line), $M_{LQ}/2$ (dot-dashed line) and $2M_{LQ}$ (dashed line). The horizontal black lines correspond to the expected limit cross section (dotted line) and the observed limit cross section (dashed line) for each coupling.